Atmos. Meas. Tech. Discuss., doi:10.5194/amt-2016-176, 2016
Manuscript under review for journal Atmos. Meas. Tech.
Published: 16 June 2016

Atmospheric Measurement Techniques
Discussions

Tropospheric delay parameters from numerical weather models for multi-GNSS precise positioning

Cuixian Lu[1], Florian Zus[1], Maorong Ge[1], Robert Heinkelmann[1], Galina Dick[1], Jens Wickert[1,2], and Harald Schuh[1,2]

[1]German Research Centre for Geosciences GFZ, Telegrafenberg, 14473 Potsdam, Germany
[2]Technische Universität Berlin, Institute of Geodesy and Geoinformation Science, 10623 Berlin, Germany

Correspondence to: Cuixian Lu (cuixian@gfz-potsdam.de)

Abstract. The recent dramatic development of multi-GNSS (Global Navigation Satellite Systems) constellations brings great opportunities and potential for more enhanced precise positioning, navigation, timing, and other applications. Significant improvement on positioning accuracy, reliability, as well as convergence time with the multi-GNSS fusion can be observed in comparison with the single-system processing like GPS (Global Positioning System). In this study, we develop a numerical weather model (NWM)-constrained PPP processing system to improve the multi-GNSS precise positioning. Tropospheric delay parameters which are derived from the European Centre for Medium-Range Weather Forecasts (ECMWF) analysis are applied to the multi-GNSS PPP, a combination of four systems: GPS, GLONASS, Galileo, and BeiDou. Observations from stations of the IGS (International GNSS Service) Multi-GNSS Experiments (MGEX) network are processed, with both the standard multi-GNSS PPP and the developed NWM-constrained multi-GNSS PPP processing. The high quality and accuracy of the tropospheric delay parameters derived from ECMWF are demonstrated through comparison and validation with the IGS final tropospheric delay products. Compared to the standard PPP solution, the convergence time is shortened by 32.0 %, 37.5 %, and 25.0 % for the north, east, and vertical components, respectively, with the NWM-constrained PPP solution. The positioning accuracy also benefits from the NWM-constrained PPP solution, which gets improved by 2.5 %, 12.1 %, and 18.7 % for the north, east, and vertical components, respectively.

Keywords. Multi-GNSS; GPS; Tropospheric delay parameters; Numerical weather models; Precise point positioning (PPP); Convergence time; Positioning accuracy.

1 Introduction

As the first space-based satellite navigation system, Global Positioning System (GPS) consisting of a dedicated satellite constellation has been extensively applied for many geodetic applications in the last decades (Ge et al., 2008; Li et al., 2013). In particular, the GPS Precise Point Positioning (PPP, Zumberge et al., 1997) technique draws special interests as it enables accurate positioning of mm to cm accuracy with a single receiver (Blewitt et al., 2006). Due to its significant advantages in terms of operational flexibility, global coverage, cost-efficiency, and high accuracy, the PPP approach has been demonstrated to be a powerful tool and it is widely used in various fields such as Precise Orbit Determination (POD) of Low Earth Orbiters (LEO), crustal deformation monitoring, precise timing, GPS meteorology, and kinematic positioning of mobile platforms (Zumberge et al., 1997; Kouba and H éroux, 2001; Gao and Shen, 2001; Zhang and Andersen, 2006; Ge et al., 2008). With the continuously improved density of the tracking network infrastructure as well as the enhanced precise satellite orbit and clock correction products with short-latency (e.g., real-time) availability, many innovative applications like geo-hazard monitoring, seismology, nowcasting of severe weather events or regional short-term forecasting based on the PPP technique have also been emerging and undergoing great developments (Larson et al., 2003; Li et al., 2013; Lu et al., 2015). However, the GPS-only PPP shows limitations concerning the convergence time, positioning accuracy, and long re-initialization period due to insufficient satellite visibility and limited spatial geometry, especially under constrained environmental conditions where the signals are blocked or interrupted.

The world of satellite navigation is going through dramatic changes and is stepping into a stage of multi-constellation GNSS (Global Navigation Satellite Systems) (Montenbruck et al., 2014). Not only is GPS of full capability and under continuous modernization, but also GLONASS has finished the revitalization and is now fully operational. Besides, two new constellations, Galileo and BeiDou, have recently emerged. The European Galileo currently comprises of 12 satellites deployed in orbit and it is working towards a fully operational stage. The Chinese BeiDou officially launched a continuous positioning, navigation, and timing (PNT) service covering the whole Asia-Pacific region at the end of 2012. It is continuously developing to a global system in the near future. In addition, the Japanese Quasi-Zenith Satellite System (QZSS) and the Indian Regional Navigation Satellite System (IRNSS) are also growing, with one and five satellites currently (as of 2016) operating in orbit, respectively. So

Atmos. Meas. Tech. Discuss., doi:10.5194/amt-2016-176, 2016
Manuscript under review for journal Atmos. Meas. Tech.
Published: 16 June 2016

Atmospheric Measurement Techniques Discussions

far, more than 80 navigation satellites can be in view and transmit data benefitting from the multi-constellation GNSS, which brings great opportunities for more precise positioning, navigation, timing, remote sensing, and other applications (Ge et al., 2012).

Undoubtedly, the integration of all existing navigation satellite systems could provide more observations and could thus enable definite improvements on reliability, positioning accuracy and convergence time of PPP in comparison with the stand-alone GPS PPP. Li et al. (2015a) developed a four-system (GPS+ GLONASS + Galileo + BeiDou) positioning model to fully exploit all available observables from different GNSS. They demonstrated that the fusion of multiple GNSS showed a significant effect on shortening the convergence time and improving the positioning accuracy when compared to single-system PPP solutions. The benefits of the four-system model were also found when applied for real-time precise positioning (Li et al., 2015b), where a reduction of the convergence time by about 70 % and an improvement of the positioning accuracy by about 25 % with respect to the GPS-only processing were illustrated. The fusion of multi-GNSS constellations has developed to be one of the hot topics within the GNSS community, not only limited to precise positioning but also for related applications. For example, the multi-GNSS PPP exhibits significant advantages for GNSS meteorology applications, such as the real-time retrieval of atmospheric parameters including integrated water vapor, tropospheric delays, and horizontal gradients, in particular for the high-temporal resolution tropospheric gradients (Li et al., 2015c; Lu et al., 2016). Therefore, to improve the performance of multi-GNSS precise positioning concerning both positioning accuracy and solution convergence, is the

Atmos. Meas. Tech. Discuss., doi:10.5194/amt-2016-176, 2016
Manuscript under review for journal Atmos. Meas. Tech.
Published: 16 June 2016

Atmospheric Measurement Techniques Discussions
Open Access
EGU

main focus of our study.

Numerical weather models (NWM) are able to provide the required information for describing the neutral atmosphere, from which the meteorological parameters can be derived at any location and at any time by applying interpolation, within the area and time window considered by the model (Pany et al., 2001). In the past, the application of NWM in space geodetic analysis mainly focused on the determination of mapping functions (Niell, 1996; Boehm et al., 2006). With respect to the improvements in spatiotemporal resolutions as well as in precision and accuracy of the NWM during recent years, tropospheric delay parameters, such as zenith total delay (ZTD), slant total delay, and tropospheric gradients, derived from the NWM could satisfy the accuracy requirements for most GNSS applications (Andrei and Chen, 2008). Data from the NWM have been used to perform tropospheric delay modeling or correct for the neutral atmospheric effects in GNSS data processing. Hobiger et al. (2008a) made use of ray-traced slant total delays derived from a regional NWM for GPS PPP within the area of Eastern Asia. They demonstrated an improvement of station coordinate repeatability by using this strategy in comparison to the standard PPP approach where the tropospheric delays were estimated as unknown parameters. Furthermore, an enhanced algorithm for extracting the ray-traced tropospheric delays of higher accuracy from the NWM in real-time mode was proposed by Hobiger et al. (2008b). The authors presented the potential and the feasibility of applying the NWM-derived tropospheric delay corrections into real-time PPP processing. Besides, Ibrahim and El-Rabbany (2011) evaluated the performance of implementing tropospheric corrections from the NOAA (National Oceanic and

Atmos. Meas. Tech. Discuss., doi:10.5194/amt-2016-176, 2016
Manuscript under review for journal Atmos. Meas. Tech.
Published: 16 June 2016

Atmospheric Administration) Tropospheric Signal Delay Model (NOAATrop) into GPS PPP. They pointed out an improvement of convergence time by about 1 %, 10 %, and 15 % for the latitude, longitude, and height components, respectively, by using the NOAA troposphere model when compared to the results achieved with the previously used Hopfield model.

In this study, we develop a NWM-constrained PPP processing method to improve the multi-GNSS (a combination of four systems: GPS, GLONASS, Galileo, and BeiDou) precise positioning. Tropospheric delay parameters, which are derived from the European Centre for Medium-Range Weather Forecasts (ECMWF, http://www.ecmwf.int/) analysis are applied to multi-GNSS PPP. Observations from the IGS (International GNSS Service) Multi-GNSS Experiments (MGEX) network are processed. The quality of tropospheric delay parameters retrieved from the ECMWF analysis is assessed by comparison with the IGS final tropospheric delay products (ftp://cddis.gsfc.nasa.gov/gnss/products/troposphere/zpd/). The performance of multi-GNSS PPP making use of the NWM-derived tropospheric delay parameters is evaluated in terms of both convergence time and positioning accuracy.

This article is organized as follows: Section 2 illustrates the IGS tracking network for MGEX, the multi-GNSS data collection, and the tropospheric delay parameters retrieved from ECMWF. Two multi-GNSS PPP processing scenarios, the standard and the NWM-constrained PPP, are presented in detail focusing on the modeling of the tropospheric delays. Thereafter, Section 3 describes the comparison of tropospheric delay parameters from ECMWF with respect to the IGS final tropospheric delay products. In Sect. 3, the positioning results, in terms of the convergence time and the positioning accuracy, achieved with the NWM-constrained multi-GNSS PPP solution are illustrated in comparison to the ones with the standard PPP solution. The conclusions and discussions are presented in Sect. 4.

2 Data collection and processing

2.1 Multi-GNSS data collection

In response to the dramatic development of the global satellite navigation world along with the upcoming systems and signals, the IGS initialized the MGEX campaign to enable a multi-GNSS service of tracking, collecting, and analyzing data of all available signals from GPS, GLONASS, BeiDou, Galileo, QZSS, and any other space-based augmentation system (SBAS) of interest (Montenbruck et al., 2014). Accordingly, a new worldwide network of multi-GNSS monitoring stations under the framework of the MGEX project has been deployed in the past two years in parallel with the IGS network, which only serves for GPS and GLONASS. Currently, the MGEX network consists of more than 120 stations, which are globally distributed and provide excellent capability of multi-GNSS constellation tracking and data delivering owing to the contributions from about 27 agencies, universities, and other institutions of 16 countries (http://igs.org/mgex). Besides the tracking of the GPS constellation, the majority of the MGEX stations enable offering the GLONASS data. At least one of the new BeiDou, Galileo, or QZSS constellations can be tracked for each MGEX station. Today, about 75 stations are capable of tracking the Galileo satellites, 80 stations are tracking the GLONASS satellites, and the

BeiDou constellation is supported by more than 30 receivers. Figure 1 shows the geographical distribution of the MGEX stations and their supported constellations, except GPS, which can be tracked by each station.

2.2 NWM data collection

The pressure, temperature, and specific humidity fields of the ECMWF operational analysis are utilized to retrieve the tropospheric delay parameters. The ECMWF data are available at the German Research Centre for Geosciences (GFZ) with a horizontal resolution of 1°×1° on 137 vertical model levels extending from the Earth's surface to about 80 km. We use the ray-trace algorithm proposed by Zus et al. (2014) and compute station specific zenith hydrostatic (non-hydrostatic) delays, derive all three hydrostatic (non-hydrostatic) mapping function coefficients (Zus et al., 2015a) and the horizontal delay gradient components (Zus et al., 2015b). The calculated station-specific tropospheric delay parameters are available every six hours per day and are valid at 0, 6, 12, and 18 UTC.

2.3 Multi-GNSS PPP processing

In the PPP processing, precise satellite orbits and clocks are fixed to previously determined values. The multi-GNSS (here GPS, GLONASS, Galileo, and BeiDou) PPP processing model can be expressed as follows,

Atmos. Meas. Tech. Discuss., doi:10.5194/amt-2016-176, 2016
Manuscript under review for journal Atmos. Meas. Tech.
Published: 16 June 2016

Atmospheric Measurement Techniques
Discussions

$$\begin{cases} l_{r,j}^{G} = -\mathbf{u}_r^{G}\cdot\mathbf{r} + t_r + \lambda_{jG}(b_{rG,j} - b_j^{G}) + \lambda_{jG}N_{r,j}^{G} - \kappa_{jG}\cdot I_{r,1}^{G} + T + \varepsilon_{r,j}^{G} \\ l_{r,j}^{R_k} = -\mathbf{u}_r^{R}\cdot\mathbf{r} + t_r + \lambda_{jR_k}(b_{rR_k,j} - b_j^{R}) + \lambda_{jR_k}N_{r,j}^{R} - \kappa_{jR_k}\cdot I_{r,1}^{R} + T + \varepsilon_{r,j}^{R} \\ l_{r,j}^{E} = -\mathbf{u}_r^{E}\cdot\mathbf{r} + t_r + \lambda_{jE}(b_{rE,j} - b_j^{E}) + \lambda_{jE}N_{r,j}^{E} - \kappa_{jE}\cdot I_{r,1}^{E} + T + \varepsilon_{r,j}^{E} \\ l_{r,j}^{C} = -\mathbf{u}_r^{C}\cdot\mathbf{r} + t_r + \lambda_{jC}(b_{rC,j} - b_j^{C}) + \lambda_{jC}N_{r,j}^{C} - \kappa_{jC}\cdot I_{r,1}^{C} + T + \varepsilon_{r,j}^{C} \end{cases} \quad (1)$$

$$\begin{cases} p_{r,j}^{G} = -\mathbf{u}_r^{G}\cdot\mathbf{r} + t_r + c\cdot d_{rG} + \kappa_{jG}\cdot I_{r,1}^{G} + T + e_{r,j}^{G}, \\ p_{r,j}^{R_k} = -\mathbf{u}_r^{R}\cdot\mathbf{r} + t_r + c\cdot d_{rR_k} + \kappa_{jR_k}\cdot I_{r,1}^{R} + T + e_{r,j}^{R} \\ p_{r,j}^{E} = -\mathbf{u}_r^{E}\cdot\mathbf{r} + t_r + c\cdot d_{rE} + \kappa_{jE}\cdot I_{r,1}^{E} + T + e_{r,j}^{E}, \\ p_{r,j}^{C} = -\mathbf{u}_r^{C}\cdot\mathbf{r} + t_r + c\cdot d_{rC} + \kappa_{jC}\cdot I_{r,1}^{C} + T + e_{r,j}^{C}, \end{cases} \quad (2)$$

where r and j refer to receiver and frequency, respectively; The capital indices G, R, E, and C refer to the satellites of GPS, GLONASS, Galileo, and BeiDou, respectively; R_k denotes the GLONASS satellite with frequency factor k; $l_{r,j}$ and $p_{r,j}$ denote the "observed minus computed" phase and pseudorange observables; $\mathbf{u}_r^s$ is the unit vector in the receiver to satellite direction; $\mathbf{r}$ denotes the vector of the receiver position increments relative to the a priori position, which is used for linearization; t_r is the receiver clock bias; $N_{r,j}$ is the integer ambiguity; b_j are the uncalibrated phase delays; λ_j is the wavelength; the ionospheric delays I_j at different frequencies can be expressed as $I_j = \kappa_j \cdot I_1, \kappa_j = \lambda_j^2 / \lambda_1^2$; and T is the slant tropospheric delay. Due to the different frequencies and signal structures of each individual GNSS, the code biases d_{rG}, d_{rR_k}, d_{rE}, and d_{rC} are different for each multi-GNSS receiver. These inter-system biases (ISB) and inter-frequency biases (IFB) of the GLONASS satellites with different frequency factors have to be estimated or corrected for a combined processing of multi-GNSS observations. $e_{r,j}$ and $\varepsilon_{r,j}$ denote the sum of measurement noise and multipath effects of pseudorange and phase observations, respectively. The phase center offsets and variations, the tidal loading, and the phase wind-up are corrected with the models according to Kouba (2009).

The slant total delay T can be described as the sum of the hydrostatic and non-hydrostatic/wet components, and the horizontal gradient components (Chen and Herring, 1997),

$$T = mf_h \cdot ZHD + mf_{nh} \cdot ZWD + mf_G \cdot (G_{ns} \cdot \cos(a) + G_{ew} \cdot \sin(a)) \quad (3)$$

where ZHD and ZWD denote the zenith hydrostatic and non-hydrostatic/wet delays, respectively, mf_h and mf_w are the hydrostatic and non-hydrostatic mapping functions (here Global Mapping Functions (GMF), Boehm et al., 2006), mf_G represents the gradient mapping function, G_{ns} and G_{ew} are the north-south (NS) and east-west (EW) delay gradients, respectively, and a is the azimuth of the line of sight of the individual observation.

Concerning the approach for tropospheric delay modeling, two PPP scenarios are applied in this study: one is the standard PPP processing with tropospheric delays estimated as unknown parameters, and the other is the developed NWM-constrained PPP algorithm which utilizes tropospheric delay parameters derived from ECMWF. For the standard PPP processing, a priori ZHD is calculated by use of the empirical models (Saastamoinen, 1973) based on the provided meteorological information (here Global Pressure and Temperature 2 model (GPT2), Lagler et al., 2013) at a given location. Owing to the high variability of the water vapor distribution, the ZWD is estimated as an unknown parameter in the adjustment together with the other parameters, such as the station coordinates. The horizontal

Atmos. Meas. Tech. Discuss., doi:10.5194/amt-2016-176, 2016
Manuscript under review for journal Atmos. Meas. Tech.
Published: 16 June 2016

Atmospheric Measurement Techniques Discussions

tropospheric gradients, G_{ns} and G_{ew}, are also estimated, both with a temporal resolution of 24 hours. The parameters estimated in the standard PPP processing include station coordinates, ambiguity parameters, receiver clock corrections, ZWD, and gradient components, all of which are adjusted in a sequential least squares filter. For the standard multi-GNSS PPP processing, the parameter vector $\mathbf{X}$ can be described as,

$$\mathbf{X} = \left(\mathbf{r}\ t_r\ ZWD\ G_{ns}\ G_{ew}\ d_{rE}\ d_{rC}\ d_{rR_k}\ \mathbf{I}_{r,1}^{s}\ \mathbf{N}_{r,j}^{s}\right)^T \tag{4}$$

For the NWM-constrained PPP approach, ZHD, hydrostatic and non-hydrostatic mapping functions are derived from the ECMWF analysis. The ZWD from ECMWF is considered as the a priori value for the wet delays, while a residual wet delay is estimated during the parameter estimation process in order to account for possible imperfections inherent in the NWM. The horizontal gradients are also derived from the ECMWF analysis and are fixed during the processing. In this approach, the unknown parameters are station coordinates, ambiguity parameters, receiver clock corrections, and the residual ZWD error. The latter is modeled as a random walk process with a priori constraints related to the accuracy of tropospheric delay parameters derived from ECMWF. Accordingly, the parameter vector $\mathbf{X}$ in the NWM-constrained multi-GNSS PPP can be expressed as,

$$\mathbf{X} = \left(\mathbf{r}\ t_r\ Resi_{ZWD}\ d_{rE}\ d_{rC}\ d_{rR_k}\ \mathbf{I}_{r,1}^{s}\ \mathbf{N}_{r,j}^{s}\right)^T, \quad Resi_{ZWD} \sim N(0, \sigma_{ZWD}^2) \tag{5}$$

where $Resi_{ZWD}$ denotes the residual ZWD error, and σ_{ZWD}^2 is the variance of the *ZWD*.

In order to carry out a rigorous multi-GNSS analysis including the estimation of the inter-system and inter-frequency biases, the observables from the four individual GNSS are processed together in a single weighted least squares estimator. For the two multi-GNSS PPP scenarios, the receiver position increment $\mathbf{r}$ is estimated as static parameter on a daily basis. The receiver clock bias t_r is estimated as white noise, and the inter-system and inter-frequency code biases are estimated as parameters on a daily basis. The ZWD or the residual wet delay $Resi_{ZWD}$ are modeled as piece-wise constant parameters (with a temporal resolution of two hours). The code biases for GPS satellites are set to zero to eliminate the singularity between receiver clock and code bias parameters. All the estimated biases of the other systems are relative to those of the GPS satellites. The phase ambiguity parameters $\mathbf{N}_{r,j}^{s}$, which absorb the phase delays b_j, are estimated as constants for each continuous arc. With the combination of the dual-frequency raw phase and pseudorange observations, the ionospheric delays $\mathbf{I}_{r,1}^{s}$ are considered as estimated parameters for each satellite-site pair and each epoch. Besides, an elevation-dependent weighting and a cut-off elevation angle of 5° are applied.

3 Results and analysis

3.1 Comparison between ECMWF and IGS ZTD

In this section, the quality of tropospheric zenith delay parameters derived from ECMWF analysis is evaluated by comparing with the zenith path delay products offered by IGS. Specifically, the ECMWF ZTD for 34 globally-distributed stations from the IGS MGEX network during September 2015 are validated by the official IGS ZTD products which are provided with a temporal resolution of five minutes. As the ECMWF ZTD are sampled every six hours, we do not interpolate in time but restrict the comparison to the ECMWF data epochs.

As typical examples, the ZTD series derived from ECMWF and IGS at stations KIRU (Kiruna, Sweden) and NNOR (New Norcia, Australia) are shown in Figure 2. The ECMWF ZTD are represented through black triangles, while the IGS ZTD are displayed by red squares. One can notice that the ECMWF ZTD show good agreement with the IGS ZTD in general. Most of the peaks in the ZTD series, which are mainly caused by rapid changes of the water vapor content above a station, are captured by ECMWF and IGS solutions.

The corresponding linear correlations between the ECMWF and the IGS ZTD at stations KIRU and NNOR are illustrated in Figure 3. It can be seen that ZTD from the two solutions are highly correlated, with the correlation coefficients being about 0.93 and 0.97, respectively. Figure 4 presents the distribution of ZTD differences between ECMWF and IGS for the two stations during the same period. One can notice that the ZTD differences mainly range from -15 to 15 mm for station KIRU, and vary between -10 and 10 mm for station NNOR. The mean biases of the ZTD differences between the two solutions are -3.52 and 3.31 mm for the two stations and the root-mean-square (RMS) values of the ZTD differences are 8.68 and 6.39 mm, respectively, showing an agreement at the mm-level.

Figure 5 illustrates the map of station specific mean biases and RMS values of ZTD differences between ECMWF and IGS for all stations. One can notice that the mean biases are within ±15 mm, and that a better agreement between the ECMWF and IGS ZTD for the high-latitude stations than for the low-latitude stations can be observed. The RMS values of the ZTD differences are less than 22 mm,

Atmos. Meas. Tech. Discuss., doi:10.5194/amt-2016-176, 2016
Manuscript under review for journal Atmos. Meas. Tech.
Published: 16 June 2016

Atmospheric Measurement Techniques Discussions

indicating a good agreement between the two solutions. Likewise, the RMS values present a significant latitude dependence, which is smaller for high-latitude stations and larger for low-latitude stations, resulting from the distribution of atmospheric water vapor content with respect to the stations' latitudes. The RMS values for stations in high-latitude regions are generally below 15 mm, while the ones for the stations in low-latitude regions can reach up to 22 mm. For an enhanced perspective, the RMS values of ZWD differences between ECMWF and IGS are shown as a function of the geographical latitudes in Figure 6, where a fitted parabola is also displayed in black. It can be clearly seen that the RMS values reveal strong dependence on geographical latitudes, which are larger in low-latitude (moist) regions and smaller in high-latitude (dry) regions.

3.2 Multi-GNSS PPP results

To investigate the performance of applying tropospheric delay parameters derived from ECMWF into multi-GNSS PPP, two PPP scenarios including the standard PPP and the NWM-constrained PPP are carried out for comparing and validating, following the data processing algorithms presented in Sect. 2.3. Observational data from stations of the IGS MGEX network (see Fig.1) in September 2015 are considered in this study.

As an example, Figure 7 illustrates the estimated north/east/up coordinates obtained from the two multi-GNSS PPP processing method at station WIND (Windhoek, Namibia, 22.57 ° S, 17.09 ° E) on September 12, 2015. As a reference, positioning results derived from the stand-alone GPS PPP are also displayed applying similar strategies as the multi-GNSS processing. The standard PPP solutions are shown by black triangles, while the NWM-constrained PPP solutions are shown by red squares. The left figures show the multi-GNSS results. One can notice that it takes about 17 min for the NWM-constrained multi-GNSS PPP to achieve an accuracy of a few centimeters for the north component, in comparison to 25 min in case of the standard PPP solution. The convergence time is shortened by about 32.0 % by using the NWM-derived tropospheric delay parameters. Meanwhile, the positioning series of the standard PPP solution show a larger jump than that of the NWM-constrained PPP solution before the convergence. As for the east component, centimeter-level accuracy is achievable with a convergence time of about 40 min for the standard vs. 25 min for the NWM-constrained PPP solution. Accordingly, the solution is improved in terms of convergence time by about 37.5 % with the NWM-constrained PPP. For the vertical component, it can be seen that the convergence time is also clearly reduced by applying the NWM-constrained PPP. A convergence time of about 20 min and 15 min is required to reach decimeter-level accuracy for the standard PPP solution and the NWM-constrained PPP solution, respectively, indicating an improvement of about 25.0 % when applying the NWM-constrained PPP. In addition, the positioning series exhibit much more jumps and fluctuations with the standard PPP solution, in particular before the solution convergence, which get significantly improved when the NWM-constrained PPP is performed.

As shown in the right figures, the positioning performance, not only the convergence time but also the positioning series, gets remarkably improved with the multi-GNSS processing (left figures) compared to the GPS-only solution. For the standard GPS PPP, an accuracy at the centimeter-level is obtainable with a convergence time of about 50 min and 60 min for the north and east components, respectively. In comparison, the convergence time is improved by about 60 % and 33.3 %, when the

Atmos. Meas. Tech. Discuss., doi:10.5194/amt-2016-176, 2016
Manuscript under review for journal Atmos. Meas. Tech.
Published: 16 June 2016

standard multi-GNSS PPP (about 20 min and 40 min for north and east components, respectively) are carried out. Meanwhile, it takes about 20 min and 40 min for the NWM-constrained GPS PPP solution to reach a comparable centimeter-level accuracy for the north and east components, respectively, shortening the solution convergence time to about the same extent as the multi-GNSS combination. In the standard GPS PPP solution, a convergence time of about 50 min is required for the vertical component to achieve an accuracy of a few decimeters, in comparison to 20 min in case of the standard multi-GNSS PPP solution. The convergence time is reduced by about 60 % attributing to the multi-GNSS fusion. The convergence time for the NWM-constrained GPS PPP solution is about 10 min for the vertical component, revealing an improvement of up to 80 % compared to the standard GPS PPP solution. In addition, it can be found that the NWM-constrained PPP reveals significant contribution to improving the positioning series of all three components, showing more stable and less fluctuated results.

In Figure 8, the statistical results of the multi-GNSS PPP solutions are presented with different session lengths (5, 8, 10, 15, 17, 20, 25, 30, 40, 50, and 60 min). The RMS values of the positioning results for the north/east/up components are calculated for selected stations from the MGEX network over a sample period from September 1 to September 30, 2015. The standard PPP solution is shown in orange, the NWM-constrained PPP solution in olive. Obviously, the positioning accuracy of each component improves along with the increase of the session length for both PPP scenarios. In general, the positioning accuracy of the north component is better than that of the east and the vertical components, while the vertical component performs the worst, which may be attributed to the

Atmos. Meas. Tech. Discuss., doi:10.5194/amt-2016-176, 2016
Manuscript under review for journal Atmos. Meas. Tech.
Published: 16 June 2016

Atmospheric Measurement Techniques
Discussions
Open Access

configuration of the satellite constellation.

For the north component, the RMS values obtained from the NWM-constrained PPP solution are smaller than the ones from the standard PPP solution at the same session length, especially before convergence. The positioning accuracy achieved with the NWM-constrained PPP is improved by about 2.5 % compared to the one with the standard PPP. Besides, a convergence time of about 20 min and 25 min is observed for the NWM-constrained PPP solution and the standard PPP solution, respectively: an improvement of about 20.0 %. In terms of the east component, higher accuracy can be found again for the NWM-constrained PPP solution, with the RMS values reduced by about 12.1 %. Meanwhile, the standard PPP solution takes about 25 min to achieve an accuracy of a few centimeters; the same level is reached in about 17 min for the NWM-constrained PPP solution, a significant reduction in the convergence time of about 32.0 %.

As for the up component, it can be noticed that the positioning accuracy achieved from the NWM-constrained PPP solution is obviously higher than that from the standard PPP solution, an improvement of about 18.7 %. More than 20 min are required for the standard PPP solution to reach an accuracy of a few decimeters, while the NWM-constrained PPP solution achieves the same accuracy in less than 15 min, indicating an improvement of more than 25 %.

4 Conclusions

We developed a NWM-constrained PPP processing system where tropospheric delay parameters derived from the ECMWF analysis were applied to multi-GNSS precise positioning. Observations of stations from the IGS MGEX network were processed, with both standard PPP and the developed NWM-constrained PPP algorithm. The accuracy of the tropospheric delays derived from ECMWF was assessed through comparisons with the IGS final tropospheric delay products at all IGS MGEX stations. The positioning performance, including convergence time and positioning accuracy, achieved with the NWM-constrained PPP were investigated. The benefits of applying tropospheric delay parameters from the NWM to improve multi-GNSS PPP were demonstrated by comparing with the standard PPP solution.

Our results show that the mean biases between the ECMWF and IGS ZTD are within ±15 mm, while the RMS values of the ZTD differences are less than 22 mm, indicating a good agreement between the two solutions. Besides, a better agreement for the high-latitude stations than for the low-latitude stations can be noticed. Both the mean biases and RMS values are smaller for high-latitude (dry) regions and larger for low-latitude (moist) regions, revealing significant latitude dependence. These may be accounted for by the distribution of atmospheric water vapor with respect to station latitudes. Furthermore, most of the peaks in the ZTD series, which are attributed to the rapid changes of the water vapor content above a given station, can be captured by both ECMWF and IGS solutions.

For the north component, it takes about17 min for the NWM-constrained multi-GNSS PPP to achieve an accuracy of a few centimeters, in comparison to 25 min for the standard PPP solution, showing an reduction of the convergence time of about 32.0 %. The centimeter-level accuracy is achieved for the east component after a convergence time of about 40 min and 25 min from the standard and the NWM-constrained PPP solutions, respectively. The convergence time is shortened by 37.5 % with the NWM-constrained PPP. For the vertical component, a convergence time of about 20 min and 15 min is required to reach decimeter-level accuracy for the standard PPP solution and the NWM-constrained PPP solution, respectively, indicating an improvement of about 25.0 % when applying the NWM-constrained PPP. Meanwhile, the positioning series get significantly improved with the NWM-constrained PPP solution, displaying less jumps and fluctuations, especially before the solution convergence and for the vertical component.

Besides, the positioning performance of the multi-GNSS processing achieves remarkable improvement compared to the GPS-only solution. In comparison with the standard GPS PPP, the convergence time is improved by about 60 %, 33.3 %, and 60 % for the north, east, and vertical components, respectively, when conducting the standard multi-GNSS PPP. Meanwhile, when the NWM-derived tropospheric delay parameters are implemented instead of the standard GPS PPP, the convergence time gets shortened to the same extent as the multi-GNSS processing (by about 60 % and 33.3 %) for the north and east components. An improvement of convergence time up to 80 % for the vertical component can also be observed. In addition, the NWM-constrained GPS PPP shows significant contribution to improving the positioning series for all three components, with much more stable and

Atmos. Meas. Tech. Discuss., doi:10.5194/amt-2016-176, 2016
Manuscript under review for journal Atmos. Meas. Tech.
Published: 16 June 2016

less fluctuated results in particular for the vertical component. According to the results, it can be concluded that the performance of precise positioning benefits greatly from the multi-GNSS fusion in comparison to the stand-alone GPS solution, which can be further improved when the tropospheric delay parameters derived from NWM are implemented to the multi-GNSS PPP processing.

Furthermore, the positioning accuracy obtained from the NWM-constrained multi-GNSS PPP solution is also improved in comparison with the standard PPP solution with the same session length, in particular before convergence. After the convergence of the solution, an improvement of positioning accuracy resulting from the NWM-constrained PPP solution of about 2.5 %, 12.1 %, and 18.7 % for the north, east, and vertical components, respectively, can be found.

In future studies, we will investigate the performance of applying tropospheric delay parameters derived from the NWM into precise positioning with other single satellite navigation systems, such as the Russian GLObal NAvigation Satellite System (GLONASS) and the Chinese BeiDou Navigation Satellite System (BDS). Another research focus is the evaluation of the accuracy and performance of different numerical weather models, in order to find the most appropriate one to improve precise GNSS positioning.

Acknowledgements. Many thanks go to the International GNSS Service (IGS) for providing multi-GNSS data and the IGS final tropospheric products. The ECMWF data are provided to GFZ via the German Weather Service (DWD).

References

Andrei, C. and Chen, R.: Assessment of time-series of troposphere zenith delays derived from the global data assimilation system numerical weather model, GPS Solut., 13(2):109-117, 2008.

Blewitt, G., Kreemer, C., Hammond, W. C., Plag, H.-P., Stein, S., and Okal, E.: Rapid determination of earthquake magnitude using GPS for tsunami warning systems, Geophys. Res. Lett., 33, L11309, doi:10.1029/2006GL026145, 2006.

Boehm, J., Niell, A., Tregoning, P., and Schuh, H.: Global Mapping Function (GMF): A new empirical mapping function based on numerical weather model data, Geophys. Res. Lett., 33, L7304, doi: 10.1029/2005GL025546, 2006.

Chen, G. and Herring, T.A.: Effects of atmospheric azimuth asymmetry on the analysis of space geodetic data, J. Geophys. Res., 102(B9), 20489-20502, doi:10.1029/97JB01739, 1997.

Gao, Y. and Shen, X.: Improving ambiguity convergence in carrier phase-based precise point positioning, In: Proceedings of ION GPS-2001, Salt Lake City, 11-14 September,1532-1539, 2001.

Ge, M., Gendt, G., Rothacher, M., Shi, C., and Liu, J.: Resolution of GPS carrier-phase ambiguities in precise point positioning (PPP) with daily observations, J. Geod., 82(7):389-399, doi:10.1007/s00190-007-0187-4, 2008.

Ge, M., Zhang, H., Jia, X., Song, S., and Wickert, J.: What Is Achievable with the Current COMPASS Constellation?, GPS World 11, 29-34, 2012.

Hobiger, T., Ichikawa, R., Takasu, T., Koyama, Y., and Kondo, T.: Ray-traced troposphere slant delays for precise point positioning, Earth Planets Space, 60(5), e1-e4, 2008a.

Hobiger, T., Ichikawa, R., Koyama, Y., and Kondo, T.: Fast and accurate ray-tracing algorithms for real-time space geodetic applications using numerical weather models, J. Geophys. Res., 113, D20302, doi:10.1029/2008JD010503, 2008b.

Ibrahim, H. and El-Rabbany, A.: Performance analysis of NOAA tropospheric signal delay model, Meas. Sci. Technol., 22:115107, doi:10.1088/0957-0233/22/11/115107, 2011.

Kouba, J. and Héroux, P.: Precise point positioning using IGS orbit and clock products, GPS Solut., 5(2):12-28, doi:10.1007/PL00012883, 2001.

Kouba, J.: A Guide to Using International GNSS Service (IGS) Products, http://igscb.jpl.nasa.gov/igscb/resource/pubs/UsingIGSProductsVer21.pdf, 2009.

Larson, K., Bodin, P., and Gomberg, J.: Using 1-Hz GPS data to measure deformations caused by the Denali fault earthquake, Science, 300, 1421-1424, 2003.

Lagler, K., Schindelegger, M., Boehm, J., Krásná, H., and Nilsson, T.: GPT2: Empirical slant delay model for radio space geodetic techniques, Geophys. Res. Lett., 40, 1069-1073, doi:10.1002/grl.50288, 2013.

Li, X., Ge, M., Zhang, Y., Wang, R., Xu, P., Wickert, J., and Schuh, H.: New approach for earthquake/tsunami monitoring using dense GPS networks, Sci. Rep., 3, 2682, 2013.

Li, X, Zhang, X., Ren, X., Fritsche, M., Wickert, J., and Schuh, H.: Precise positioning with current multi-constellation Global Navigation Satellite Systems: GPS, GLONASS, Galileo and BeiDou.

Sci Rep., 5, 8328, 2015a.

Li, X. Ge, M., Dai, X., Ren, X., Fritsche, M., Wickert, J., and Schuh, H.: Accuracy and reliability of multi-GNSS real-time precise positioning: GPS, GLONASS, BeiDou, and Galileo, J. Geod., 89(6), 607-635, doi:10.1007/s00190-015-0802-8, 2015b.

Li, X., Zus, F., Lu, C., Dick, G., Ning, T., Ge, M., Wickert, J., and Schuh, H.: Retrieving of atmospheric parameters from multi-GNSS in real time: Validation with water vapor radiometer and numerical weather model, J. Geophys. Res. Atmos., 120, 7189-7204. doi: 10.1002/2015JD023454, 2015c.

Lu, C., Li, X., Nilsson, T., Ning, T., Heinkelmann, R., Ge, M., Glaser, S., and Schuh, H.: Real-time retrieval of precipitable water vapor from GPS and BeiDou observations, J. Geod., 89(9), 843-856, doi:10.1007/s00190-015-0818-0, 2015.

Lu, C., Li, X., Li, Z., Heinkelmann, R., Nilsson, T., Dick, G., Ge, M., and Schuh, H.: GNSS tropospheric gradients with high temporal resolution and their effect on precise positioning, J. Geophys. Res. Atmos., 121, 912-930, doi:10.1002/2015JD024255, 2016.

Montenbruck, O., Steigenberger, P., Khachikyan, R., Weber, G., Langley, R.B., Mervart, L., and Hugentobler, U.: IGS-MGEX: preparing the ground for multi-constellation GNSS science, Inside GNSS, 9 (1), 42-49, 2014.

Niell, A. E.: Global mapping functions for the atmosphere delay at radio wavelengths, J. Geophys. Res., 101(B2), 3227-3246, 1996.

Pany, T., Pesec, P., and Stangl, G.: Elimination of tropospheric path delays in GPS observations with the

Atmos. Meas. Tech. Discuss., doi:10.5194/amt-2016-176, 2016
Manuscript under review for journal Atmos. Meas. Tech.
Published: 16 June 2016

ECMWF numerical weather model, Phys Chem Earth A 26(6-8):487-492, 2001.

Saastamoinen, J.: Contributions to the theory of atmospheric refraction - Part II. Refraction corrections in satellite geodesy, Bull. Géod., 47(1), 13-34, doi:10.1007/BF02522083, 1973.

Zhang, X. and Andersen, O.: Surface ice flow velocity and tide retrieval of the amery ice shelf using precise point positioning, J. Geod., 80(4):171-176, doi:10.1007/s00190-006-0062-8, 2006.

Zumberge, J.F., Heflin, M.B., Jefferson, D.C., Watkins, M.M., and Webb, F.H.: Precise point positioning for the efficient and robust analysis of GPS data from large networks, J. Geophys. Res., 102(B3):5005-5017, 1997.

Zus, F., Dick, G., Dousa, J., Heise, S., and Wickert, J.: The rapid and precise computation of GPS slant total delays and mapping factors utilizing a numerical weather model, Radio Sci., 49, 207-216, doi:10.1002/2013RS005280, 2014.

Zus, F., Dick, G., Dousa, J., and Wickert, J.: Systematic errors of mapping functions which are based on the VMF1 concept, GPS Solut., 19(2), 277-286, 2015a.

Zus, F., Dick, G., Heise, S., and Wickert, J.: A forward operator and its adjoint for GPS slant total delays, Radio Sci., 50, 393-405, doi:10.1002/2014RS005584, 2015b.

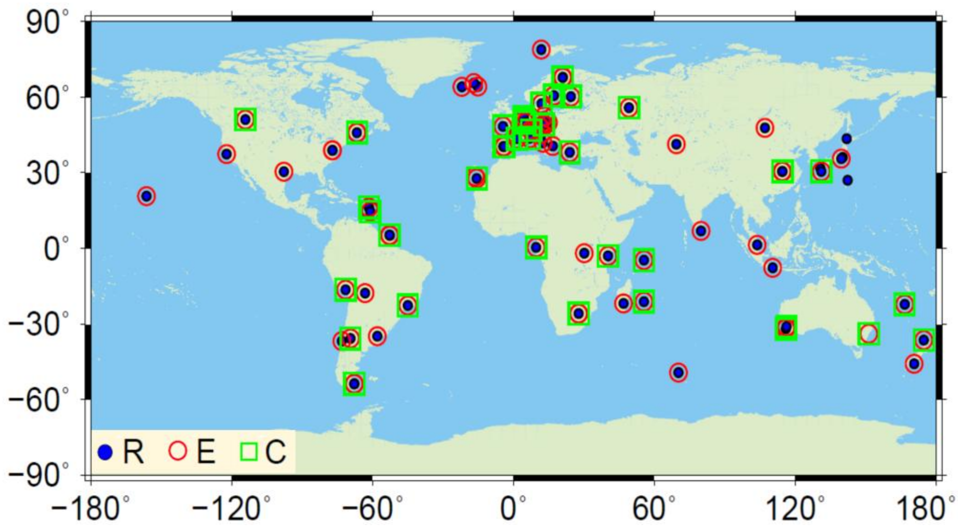

Figure 1: The geographical distribution of the MGEX stations and their supported navigation satellite constellations. The symbols "R", "E", and "C" refer to GLONASS, Galileo, and BeiDou, respectively, while GPS can be tracked by each station.

Atmos. Meas. Tech. Discuss., doi:10.5194/amt-2016-176, 2016
Manuscript under review for journal Atmos. Meas. Tech.
Published: 16 June 2016

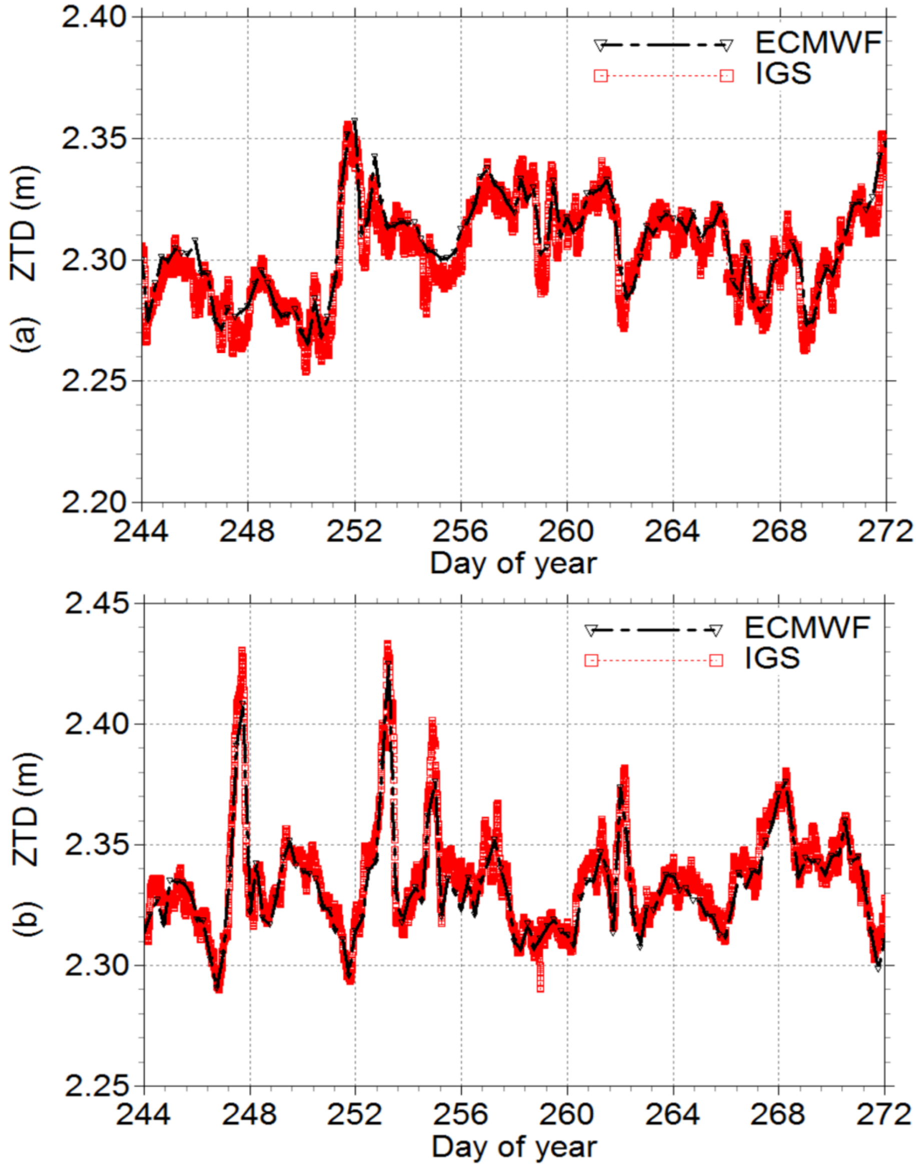

Figure 2. The time series of ECMWF and IGS ZTD at stations KIRU (a) and NNOR (b) for September (day of year (DOY) 244-272) 2015. The ECMWF ZTD are shown by black triangles, while the IGS ZTD are displayed by red squares.

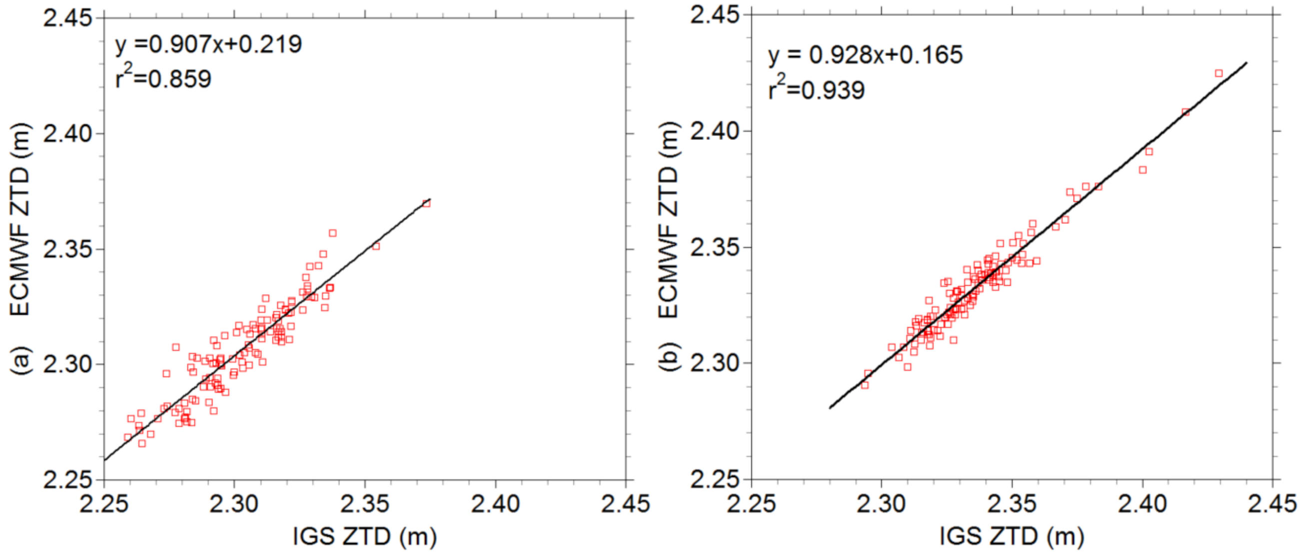

Figure 3. Scattergram of ECMWF and IGS ZTD at stations KIRU (a) and NNOR (b). The vertical and horizontal axes show ECMWF and IGS ZTD (m), respectively. The correlation coefficients (r) and the results of a linear regression are also displayed.

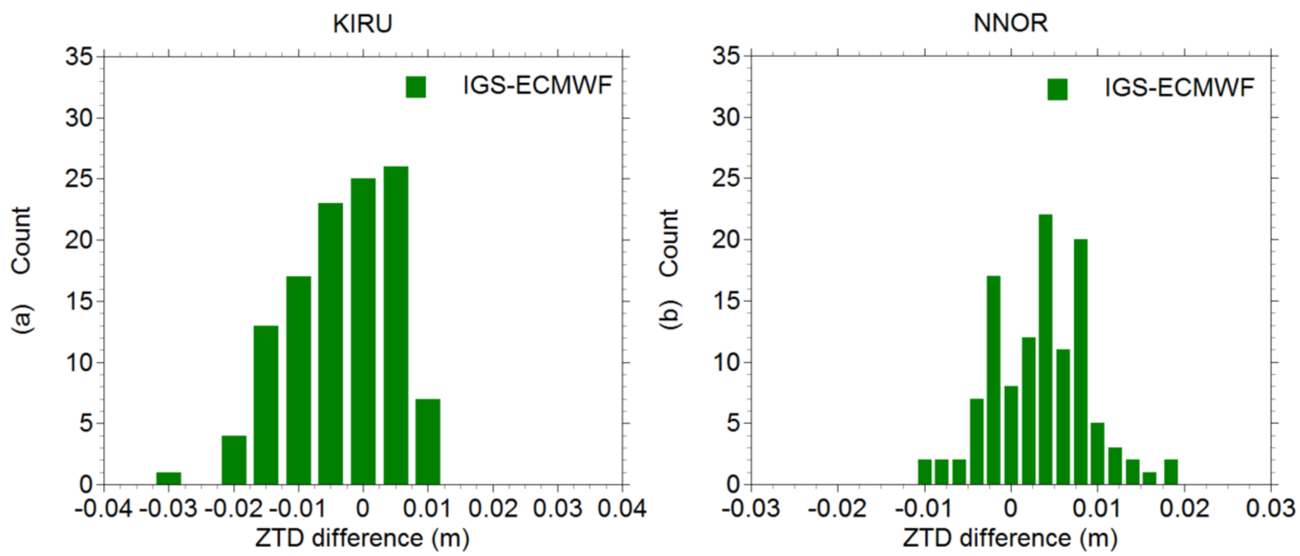

Figure 4. Distribution of ZTD differences between ECMWF and IGS ZTD at stations KIRU (a) and NNOR (b) for DOY 244-272, 2015.

Atmos. Meas. Tech. Discuss., doi:10.5194/amt-2016-176, 2016
Manuscript under review for journal Atmos. Meas. Tech.
Published: 16 June 2016

Atmospheric Measurement Techniques Discussions

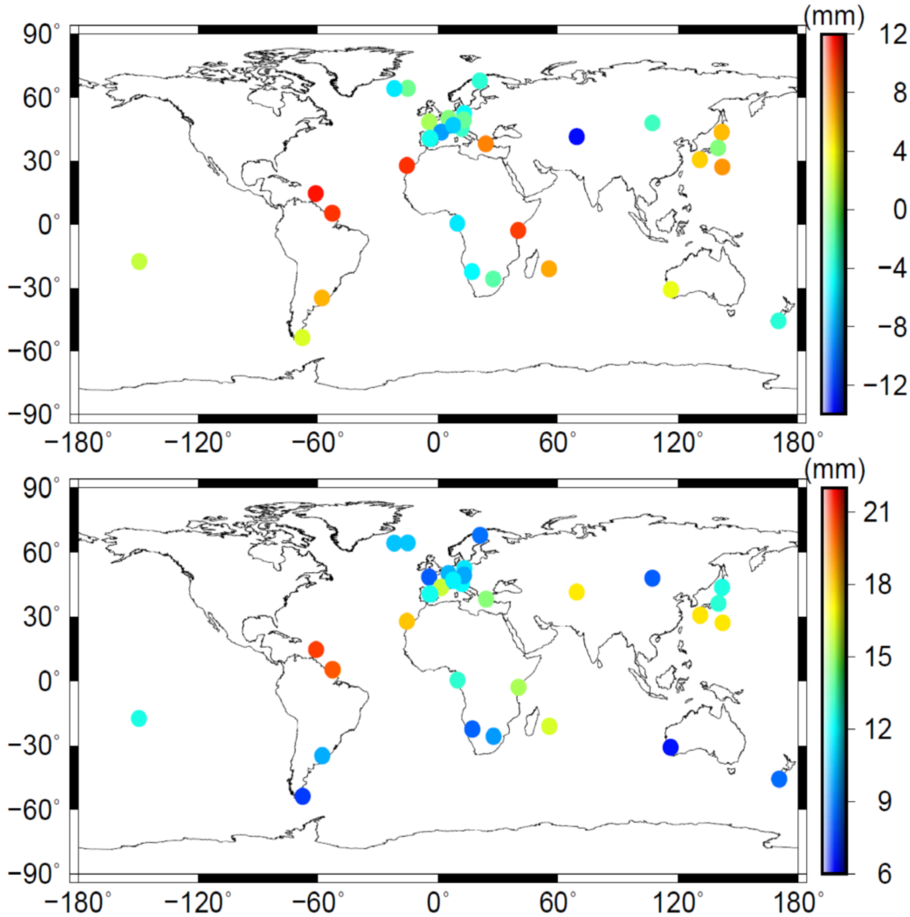

Figure 5. The map of the station-specific mean biases (top) and RMS values (bottom) of ZTD differences between ECMWF and IGS for DOY 244-272, 2015.

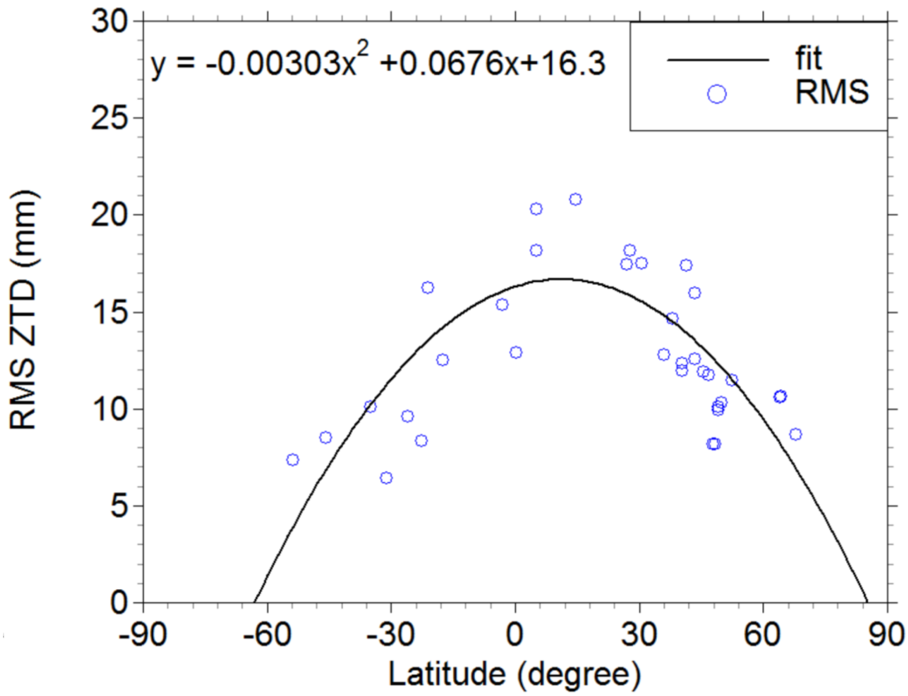

Figure 6. The RMS values of ZTD differences between ECMWF and IGS as a function of geographical latitudes. A fitted second-order polynomial is also shown in black.

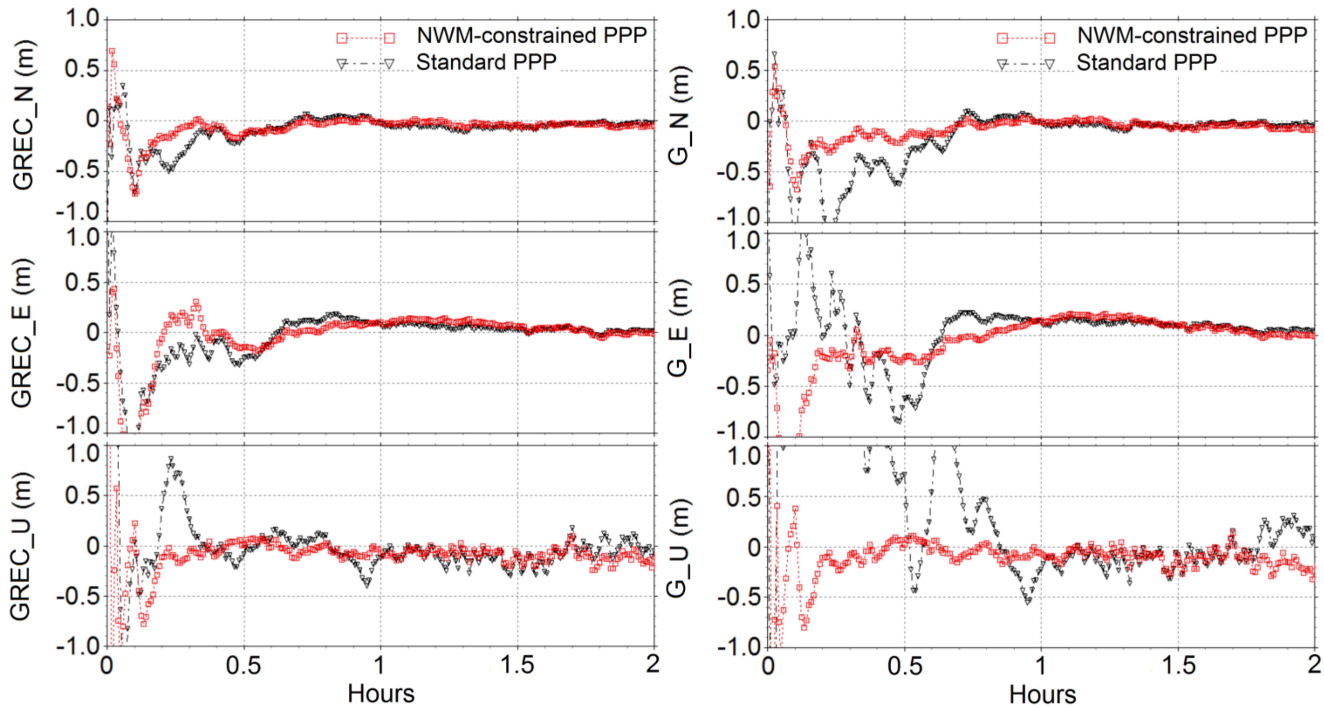

Figure 7. The multi-GNSS PPP ("GREC") solution (left) and the stand-alone GPS PPP ("G") solution (right) at station WIND (Windhoek, Namibia, 22.57 °S, 17.09 °E) on September 12, 2015 (DOY 255 of 2015). The standard PPP solutions are shown by black triangles, while the NWM-constrained PPP solutions are shown by red squares.

Atmos. Meas. Tech. Discuss., doi:10.5194/amt-2016-176, 2016
Manuscript under review for journal Atmos. Meas. Tech.
Published: 16 June 2016

Atmospheric Measurement Techniques
Discussions

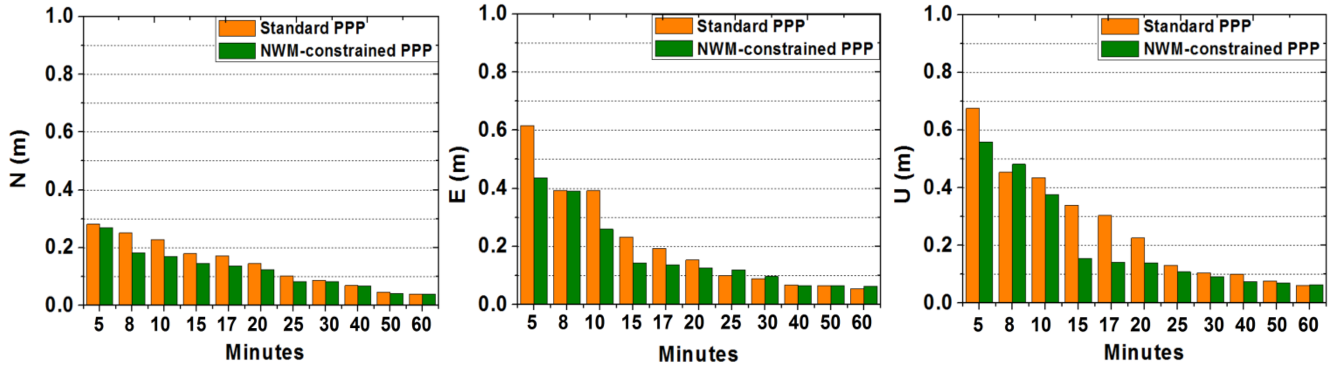

Figure 8. The RMS values for the north/east/up components with multi-GNSS PPP solution, showing at different session lengths (5, 8, 10, 15, 17, 20, 25, 30, 40, 50, and 60 min) for selected MGEX stations from September 1 to September 30, 2015. The standard PPP solution is shown in orange, the NWM-constrained PPP solution in olive.